

Melting Points and Formation Free Energies of Carbon Compounds with Sodalite Structure

Kazuhiro Sano and Kenshin Nato

Department of Physics Engineering, Mie University, Tsu, Mie 514-8507, Japan

Using first-principles calculations, we investigate the melting temperatures T_m and formation free energy of carbon compounds with sodalite structures, XC_6 , XC_{10} , and XC_{12} , where X is F, Na, Cl, and so on. These compounds are expected to be phonon-mediated superconductors exhibiting high transition temperatures T_c of up to about 100 K. We estimate T_m as a function of pressure P by using the first-principles molecular dynamics method and show the results as phase diagrams on the P - T plane together with the results of T_c . It indicates that the T_m of NaC_6 , which has a T_c up to about 100 K, is about 1300 K or more at $P = 30$ GPa. Furthermore, the T_m of FC_6 is about 2200 K even at $P = 0$ GPa, where its T_c is about 80 K. Similar results are obtained for FC_{10} and ClC_{10} systems. These results suggest that some compounds can stably exist as high-temperature superconductors even at room temperature and pressure. To examine the feasibility of synthesizing these compounds, we estimate the formation enthalpies and formation free energies. These results suggest that NaC_6 could be formed under a sufficiently high pressure of about 300 GPa and a high temperature of about 6500 K.

1. Introduction

Since the high-temperature superconductivity (HTS) of hydrogen compounds with a sodalite structure such as YH_6 and lanthanum decahydride (LaH_{10})¹⁻⁷ is predicted to indicate T_c over 250K, much effort has been made to clarify its superconductivity and/or to find new hydrogen compounds.¹⁻⁷ Based on these theoretical results,¹⁻⁵ experiments⁸⁻¹¹ succeeded in finding these superconductors whose T_c is almost close to the result of first-principles calculations. This HTS is caused by the phonon-mediated attraction, and the mechanism of the superconductivity is conventional. Therefore, T_c is determined mainly by two parameters: the electron-phonon coupling constant λ and the characteristic phonon frequency ω_{log} . When both parameters are large simultaneously, HTS can be expected. In fact, many hydrogen compounds with a sodalite structure have a large electron-phonon coupling constant λ , which is larger than about 2.0.¹⁻⁶ Typical values of ω_{log} are around 1000 K.

In these hydrogen compounds, high pressure may stabilize these characteristic structures and lead to a high phonon frequency. These materials are only stable over a limited pressure and the phonon frequency decreases with pressure.¹⁻⁶ Therefore, hydrogen compound HTS can only be achieved with devices using diamond anvil cells at this stage. To realize practical devices, the required pressure should be as low as possible, preferably normal pressure.

A material constructed with carbon atoms such as diamond has a high phonon frequency up to about 2000K at atmospheric pressure. Boron-doped diamond has been studied as a candidate of phonon-mediated HTS, and its T_c reaches ~ 25 K at atmospheric pressure.¹²⁻¹⁵ Intercalated graphite and alkali-doped C_{60} compounds are known carbonate superconductors with high T_c up to ~ 33 K.¹⁶⁻¹⁹

On the basis of the intuitive idea that the sodalite

structure plays an important role in HTS, carbon compounds with a sodalite structure have been proposed as candidates for HTS.²⁰⁻²⁵ Based on the density functional theory, materials composed only of carbon atoms are known to be insulators with a large charge gap.²⁶ By combining them with another element, X , to form a compound, carriers are introduced into the system,²²⁻²⁵ where X is Li, Na, Cl, and so on. The crystal structures of the compounds are shown in Fig. 1, where (a) XC_6 and (b) XC_{10} are shown as representative examples. XC_{12} has a structure similar to that of XC_6 shown in Fig. 1(a), except for one X atom.

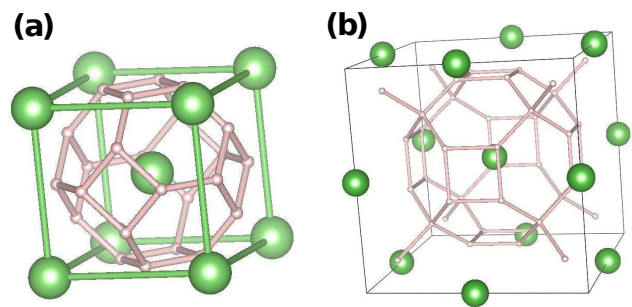


Fig. 1. (Color online) Structures of the sodalite-type compounds (a) XC_6 and (b) XC_{10} , where large spheres represent ‘ X ’-atoms and small spheres are carbon. Here, the crystal structure of XC_{12} corresponds to (a) with one X atom removed.

By first-principles calculations, it has been shown that some of these compounds exhibit T_c of about 100 K even at atmospheric pressure.^{20,22-25} However, the existence of XC_6 , XC_{10} , and XC_{12} has not yet been experimentally demonstrated. Furthermore, their stabilities at finite temperatures have not yet been clarified. Even if

these are stable near $T = 0$, they will not be practical if the crystals become unstable below room temperature.

In this study, we investigate the stability of carbon compounds with sodalite structure by the first-principles molecular dynamics (FPMD) method. First, we estimate the temperature T_u at which the system becomes unstable. Then, we estimate T_m using the known relationship between T_u and the melting point T_m . These results are shown as phase diagrams for compounds on the P - T plane, together with the superconducting transition temperature T_c .

We also calculate the formation energies of compounds from the ground state energies of the elements. To consider the effect of finite temperature, we obtain the free energies of NaC_6 and FC_6 as typical cases. From these results, we estimate the Gibbs free energies and discuss whether the formation of these compounds is possible.

2. Model and Methods

Calculations are performed using the 'Quantum ESPRESSO'(QE), which is an integrated software of open-source computer codes for electronic-structure calculations.²⁷⁾ In the FPMD calculations, we use the $N, P, T = \text{const.}$ ensemble system, where the system is a supercell made up of multiple unit cells, as shown in Fig. 1. To reduce finite size effects, the direction vector that determines the shape of the supercell is set to change at each time step of the simulation. This variable cell method includes system fluctuations better than the method using fixed direction vectors.

To estimate T_m , we use a combination of FPMD method and the Z-method,²⁸⁾ which is widely used to determine melting points.²⁹⁻³¹⁾ Our method uses FPMD simulations to determine the critical temperature T_u at which the crystal becomes thermally unstable, and then calculates T_m from the relationship $T_m \simeq T_u/1.23$.²⁸⁾ Details of the Z-method are discussed in Appendix A.

When the temperature of a system exceeds T_u , the motion of atoms in the system changes significantly in a short period of time. Therefore, it is easy to find T_u in the simulation. To obtain T_u , we calculate the Lindemann parameter defined as $L_p = \sqrt{\langle r_i^2 \rangle / d}$.³²⁻³⁴⁾ Here, r_i is the displacement of each atom from its equilibrium position at $T = 0$, and d is the distance between the nearest-neighbor atoms in the crystal at $T = 0$. The thermal average is taken over all atoms at each time step in the simulation.

When the value of L_p exceeds a certain critical value, the system becomes unstable rapidly.³⁵⁾ Thus, we calculate L_p as a function of temperature and find T_u from the point where it changes significantly.

At first, we consider the diamond system to test the above method. In Fig. 2, we show the Lindemann parameter $L_p(t)$ as a function of simulation time t for a diamond system with $N = 64$ at $P = 0\text{GPa}$, where N is the number of atoms in the system. Here, solid circles and empty circles represent the results for $T = 6000$, and 7000 K, respectively. It indicates that the values of $L_p(t)$ at $T = 6000$ K are almost constant with t , those at $T = 7000$ K increase with t and seem to diverge for $t \gtrsim 170\text{fs}$. This result suggests that T_u is between 6000

and 7000 K.

To analyze T_u in more detail, we define \bar{L}_p as the average value of $L_p(t)$ at the last four points ($t = 180, 190, 200$, and 210 fs), as shown in Fig. 2. As shown in the figure, it is expected that the system will reach a certain degree of equilibrium after about 150 fs. Therefore, we use \bar{L}_p as the approximate equilibrium value of $L_p(t)$.

Figure 3 shows \bar{L}_p as a function of T for the systems with $N = 8$ (solid circles) and 64 (empty circles). The value of \bar{L}_p increases with temperature and appears to diverge above $\bar{L}_p \sim 0.3$.³⁵⁾ Hereafter, we assume the temperature corresponding to $\bar{L}_p = 0.3$ to be T_u , where the point of $\bar{L}_p = 0.3$ is determined by interpolation. As shown in the figure, we find that $T_u \simeq 4500$ K for $N = 8$ and 6800 K for $N = 64$. This leads to $T_m \simeq 3700$ K for $N = 8$ and 5500 K for $N = 64$. When the system is small, fluctuations of the system are large and T_u tends to be low.

In Fig. 4, we show T_m of diamond as a function of pressure P along with previous theoretical^{36,37)} and experimental^{38,39)} results. Here, the solid and empty circles represent the results for $N = 8$ and 64 , respectively. In the FPMD calculation, we use mesh number $k = 4$

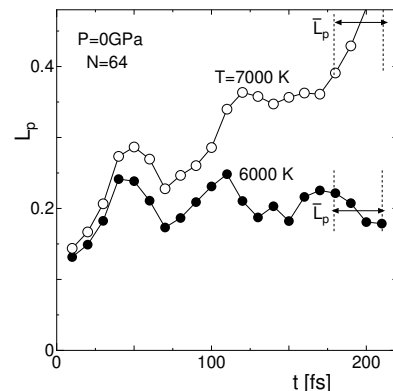


Fig. 2. Lindemann parameter L_p as a function of simulation time t , where solid circles and empty circles represent the results for $T = 6000$ and 7000 K, respectively. \bar{L}_p represents the average of the last four points of L_p .

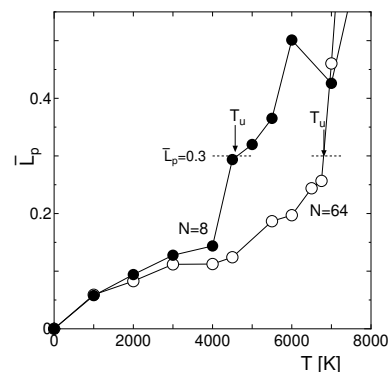


Fig. 3. \bar{L}_p as a function of T , where solid circles and empty circles represent the results for $N = 8$ and 64 , respectively. T_u is determined by the condition $\bar{L}_p = 0.3$.

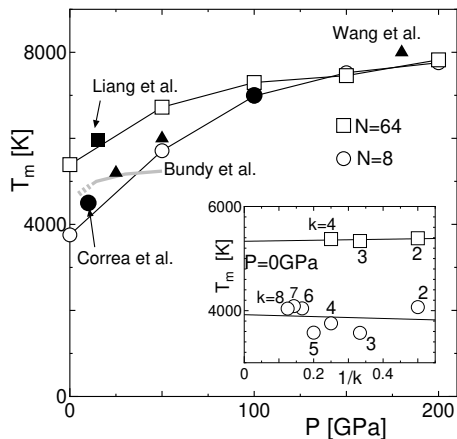


Fig. 4. Melting points of diamond as a function of pressure P , where empty circles and empty squares represent T_m for the $N = 8$ and 64 systems, respectively. Solid squares, solid circles, and solid triangles represent the results of Liang et al.,³⁹⁾ Correa et al.,³⁷⁾ and Wang et al.,³⁶⁾ respectively. The light and broken lines show the result of Bundy et al.,³⁸⁾ where the broken line indicates the phase boundary between graphite and diamond. The inset shows the k -dependence of T_m at $P = 0$ GPa, where k is the mesh number in wavenumber space.

and 2 in wavenumber space for the systems with $N = 8$ and 64, respectively. The obtained results are almost in agreement with those of previous works.

The figure also shows that the size effect for T_m is greatest when $P = 0$ and decreases as the pressure increases. This is probably due to the decrease in the fluctuations of the system with increasing pressure. The inset shows the k -dependence of T_m for the systems with $N = 8$ and 64 at $P = 0$. This indicates that the k -dependence is rather small compared with the size effect in both systems.

3. Results and Discussion

3.1 T_m as a function of P for C_6 and C_{10}

We apply the above method to pure carbon systems C_6 and C_{10} as reference systems for XC_6 and XC_{10} . In Fig. 5(a), we show the T_m of C_6 as a function of pressure P , where empty circles, empty squares, and solid triangles represent the results for $N = 12, 48,$ and 96, respectively. The T_m of C_6 is at least 2000 K at $P = 0$ and increases slightly with pressure. Although its T_m is lower than that of diamond, it is stable at room temperature and pressure.

The figure indicates that the T_m for each size is almost in agreement with each other at all pressures, and the size dependence seems to be not so large. However, the size effect of T_m is not simple. At a certain pressure, T_m is high when the size is large. However, the opposite also appears depending on the pressure. The use of variable supercells is speculated to be the cause of the complex size effects.

Figure 5(b) shows the T_m of C_{10} as a function of pressure P , where solid circles and solid squares represent the results for $N = 10$ and 40, respectively. The T_m is about 3500 K at $P = 0$ and increases slightly with pressure up to about 100 GPa, but decreases above that. This

suggests that C_{10} would be able to exist stably at room temperature and pressure, although it has not yet been experimentally discovered.

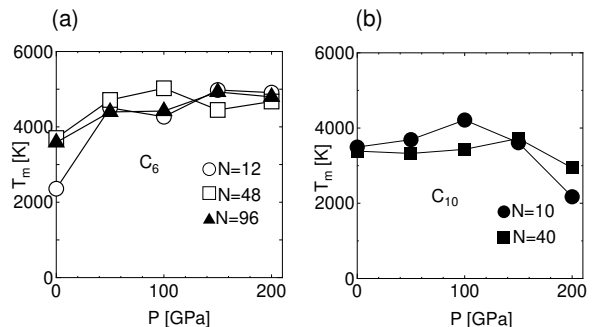


Fig. 5. (a) T_m of C_6 as a function of P , where empty circles, empty squares, and solid triangles represent T_m for the $N = 12, 48,$ and 96 systems, respectively. (b) T_m of C_{10} as a function of P , where solid circles and solid squares represent T_m for the $N = 10$ and 40 systems, respectively.

3.2 T_m and T_c as functions of P for XC_6 and XC_{10}

We consider compounds of XC_6 and XC_{10} combining carbon and X -atoms. Mainly, we present the results for compounds NaC_6 , FC_6 , FC_{10} , and ClC_{10} as typical cases.

In Fig. 6(a), we show the T_m of NaC_6 as a function of pressure P , where solid circles and solid squares represent the results for $N = 14$ and 56, respectively. In addition to T_m , the superconducting transition temperature T_c ^{40,41)} as a function of pressure P is also shown as empty circles, where T_c is multiplied by 10 for ease of viewing. Here, T_c is calculated by the tetrahedron method,²⁷⁾ which is more stable than the interpolation method²⁷⁾ in estimating T_c and removes the ambiguity in the choice of Gaussian broadening.

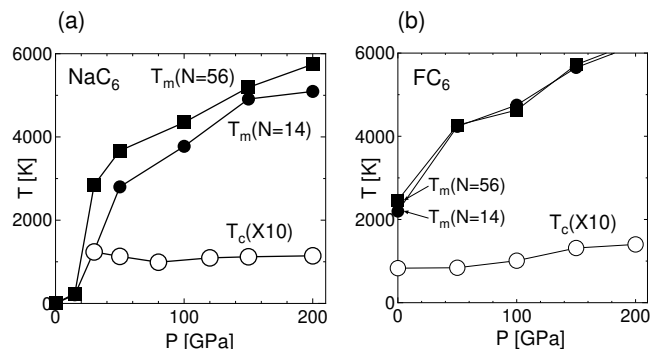


Fig. 6. (a) T_m and T_c of NaC_6 as functions of P , where solid circles and solid squares represent T_m for the $N = 14$ and 56 systems, respectively. Here, empty circles represent $T_c \times 10$. (b) T_m and T_c of FC_6 as functions of P , where solid circles and solid squares represent T_m for the $N = 14$ and 56 systems, respectively.

We find that the T_m of NaC_6 is zero and unstable at $P = 0$. However, T_m is about 2,000 K at $P = 30$ GPa and increases with pressure, reaching about 5,000

K at $P = 200$ GPa. This result seems to be consistent with those of previous works showing that NaC_6 is dynamically unstable for $P \lesssim 30$ GPa.^{22,23}) On the other hand, T_c is calculated as 149, 123, and 113 K at $P=20, 30,$ and 50 GPa, respectively. As the pressure decreases, the melting point decreases and the system becomes unstable. However, T_c appears to increase with decreasing pressure for $P \lesssim 50$ GPa.

Figure 6(b) shows the T_m of FC_6 as a function of pressure P , where solid circles and solid squares represent the results for $N = 14$ and 56 , respectively. In this case, T_m is ~ 2000 at $P = 0$ and increases with pressure and exceeds 6000 K at $P = 200$ GPa. Unlike NaC_6 , FC_6 is stable even at room temperature and pressure. T_c is 83 K at $P = 0$ and increases slightly with pressure. In a previous study, FC_6 was shown to be dynamically unstable by an interpolation method.²²) However, this is not the case in the tetrahedron method and we can obtain T_c for FC_6 .

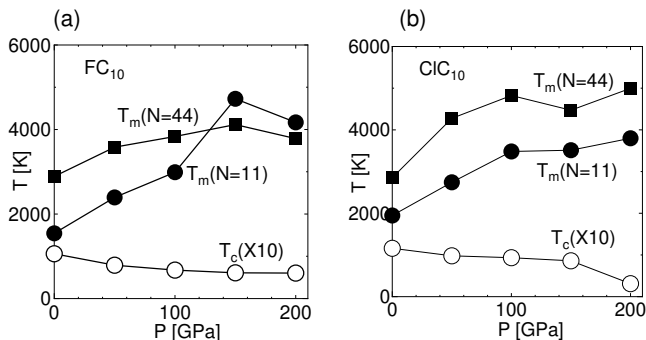


Fig. 7. (a) T_m and T_c of FC_{10} as functions of P , where solid circles and solid squares represent T_m for the $N = 11$ and 44 systems, respectively. Here, empty circles represent $T_c \times 10$. (b) T_m and T_c of ClC_{10} as functions of P , where solid circles and solid squares represent T_m for the $N = 11$ and 44 systems, respectively.

In Fig. 7(a), we show the T_m of FC_{10} as a function of pressure P , where solid circles and solid squares represent the results for $N = 11$ and 44 , respectively. Similar to Fig. 6, T_c as a function of pressure P is also shown as empty circles. Although the size dependence will be somewhat large in this case, T_m may be about 2000 K at $P = 0$. The figure also shows that T_m increases with pressure and reaches a maximum at about $P = 150$ GPa. On the other hand, T_c is about 110 K at $P = 0$ and decreases with increasing pressure. This material is also expected to exhibit superconductivity under normal pressure, similar to FC_6 .

Figure 7(b) shows the T_m of ClC_{10} as a function of pressure P , where solid circles and solid squares represent the results for $N = 11$ and 44 , respectively. Empty circles represent $T_c \times 10$. In this system, the behaviors of T_m and T_c are similar to those of FC_{10} .

For detailed data on NaC_6 , FC_6 , FC_{10} , and ClC_{10} , Table I gives T_m , T_c , λ , and ω_{\log} , where the numbers in parentheses are pressure in GPa. Here, the T_m are for the $N = 14$ system for XC_6 and for the $N=11$ system for XC_{10} .

Table I. T_m , T_c , λ , and ω_{\log} for NaC_6 , FC_6 , FC_{10} , and ClC_{10} .

P [GPa]	NaC_6 (30)	NaC_6 (200)	FC_6 (0)	FC_6 (200)
T_m [10^3 K]	1.3	5.1	2.2	6.2
T_c [K]	124	114	83	140
λ	3.81	1.76	1.37	1.45
ω_{\log} [K]	407	744	731	830
P [GPa]	FC_{10} (0)	FC_{10} (200)	ClC_{10} (0)	ClC_{10} (200)
T_m [10^3 K]	1.5	4.2	1.9	3.8
T_c [K]	92	54	98	31
λ	1.78	1.13	2.07	0.67
ω_{\log} [K]	697	653	662	997

Results for other compounds at $P = 0$ are shown in Table II. For T_m , we present the $N = 14$ system for XC_6 , the $N = 11$ system for XC_{10} , and the $N = 13$ system for XC_{12} . The table shows that XC_6 has a relatively high T_c , but T_m is not high. On the other hand, XC_{10} and XC_{12} have high T_m , but T_c is low. These results suggest that T_c decreases as the proportion of X atoms in the system decreases. This can be interpreted as a reduction in effective carriers that the X atom brings to the system.²²) This leads to a decrease in T_c . Conversely, an increase in the number of the effective carriers reduces the stability of the system and decreases T_m .

Table II. T_m , T_c , λ , and ω_{\log} for other compounds at $P = 0$.

	HC_6	LiC_6	BC_6	OC_6	ClC_6	HC_{10}
T_m [10^3 K]	0.30	0.11	0.17	0.51	0.18	2.2
T_c [K]	43	57	20	52	73	14
λ	0.75	3.47	2.37	1.23	1.14	0.53
ω_{\log} [K]	889	209	113	532	825	902
	OC_{10}	NaC_{10}	BC_{12}	NaC_{12}	FC_{12}	ClC_{12}
T_m [10^3 K]	1.5	1.3	0.57	1.2	3.0	1.7
T_c [K]	32	13	6	32	17	21
λ	0.95	0.57	0.53	0.73	0.58	0.60
ω_{\log} [K]	463	670	336	765	955	951

3.3 Formation enthalpies at $P = 0$ and $T = 0$

From the perspective of actually synthesizing these compounds, not only T_m but also the formation enthalpy may be important. We define the formation enthalpy ΔH such as $\Delta H = H_{\text{NaC}_6} - (H_{\text{Na}} + 6H_{\text{gra}})/7$ for NaC_6 , and similarly for other compounds. Here, H_{NaC_6} , H_{Na} , and H_{gra} are the enthalpies at $T = 0$ per atom of NaC_6 , sodium, and graphite, respectively. Note that the definition of ΔH given here is insufficient to estimate an exact value of the formation enthalpy. To obtain this, it is necessary to compare the energies of all compounds that contain the elements in the target compound in any ratio. Since this is very difficult in practice, we estimate ΔH as information that is useful for synthesizing compounds.

In Fig. 8, we show the ΔH of XC_6 , XC_{10} , and XC_{12} at $P = 0$, where the horizontal axis is the fraction of carbon contained in compounds. Here ΔH of XC_6 is represented

by empty circles, that of XC_{10} by empty squares, and that of XC_{12} by empty triangles. In addition, there is the ΔH of X -atom doped diamond (denoted X -diamond), in which one carbon atom in a diamond supercell made up of eight atoms is replaced by an X -atom. These are represented by solid diamonds in the figure. The solid triangle stands for the result of the graphite intercalation compound that has sodium between the layers (Na-GIC).¹⁸⁾ Each point of ΔH is accompanied by a value of T_m in units of 10^3 K. The T_m for XC_6 , XC_{10} , and XC_{12} correspond to those for the systems with $N = 14$, 11, and 13, respectively.

For reference, the formation enthalpies per atom of graphite, pure diamond, C_6 , C_{10} , and C_{60} have also been added, where these are represented by solid circles. Here, T_m^E stands for the experimental melting temperature, T_m^* is the melting temperature at the triple point near 12 GPa, and T_d^E is the decomposition temperature observed in the experiment.⁴²⁾ The results for XC_6 and XC_{12} almost agree with those of the others.²¹⁾

Comparing the difference in the value of ΔH with other studies,⁴³⁾ we find that it is about 0.008 eV for diamond and about 0.012 eV for C_{60} . For compounds NaCl, B_4C , and Be_2C ,⁴³⁾ this difference is about 0.16, 0.005, and 0.11 eV, respectively, although not shown in the figure. For XC_6 and XC_{12} , the discrepancy between our results and others' is roughly 0.06 eV.²¹⁾ In the case of compounds, the discrepancy of ΔH does not seem to be very small.

The figure shows that the ΔH of C_{60} is about 0.4 eV and close to that of C_6 . C_{60} is a material well known as fullerene and can now be synthesized. Therefore, it may be expected that the synthesis of C_6 is possible.

Unfortunately, XC_6 has low T_m , except for FC_6 and OC_6 , and may be unstable at room temperature. On the other hand, XC_{10} and XC_{12} have higher T_m than XC_6 , even though their ΔH values are similar to each other. The value of ΔH for B-diamond is about 0.25 eV, which

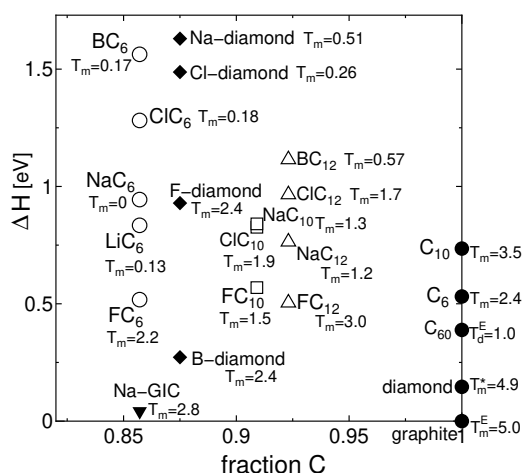


Fig. 8. The formation enthalpies, ΔH as a function of the fraction of carbon in compounds with T_m , where the unit of T_m is 10^3 K. Here, X -diamond means that one atom is replaced by X -atom in the 8-sites diamond cell, and Na-GIC represents a graphite intercalation compound with sodium between the layers.

is small, where its T_c is calculated as 32 K. This result seems to be related to the fact that boron doped diamond was found to be superconductor in experiments.^{12, 14, 15)} On the other hand, the ΔH of F-, Cl-, and Na-diamonds is around 1 eV or larger. This might correspond to the fact that superconducting diamonds doped with these elements have not been found.

The Na-GIC(sodium intercalated graphite)¹⁸⁾ considered here has the same crystal structure as the experimentally discovered Li-GIC (lithium intercalated graphite).⁴³⁾ This type of Na-GIC has not been found experimentally. However, it is an interesting isomer of NaC_6 with the sodalite structure, since finite T_c is found theoretically.¹⁸⁾

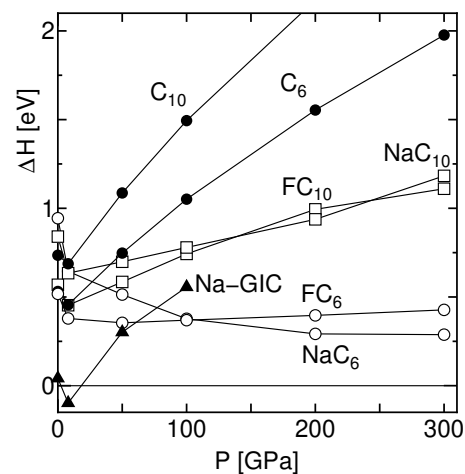


Fig. 9. ΔH as a function of P for C_6 , C_{10} , FC_6 , NaC_6 , FC_{10} , NaC_{10} , and Na-GIC.

3.4 Formation enthalpies as a function of P at $T = 0$

The pressure dependence of formation enthalpies is also interesting. In Fig. 9, we show ΔH as a function of P for C_6 , C_{10} , FC_6 , NaC_6 , FC_{10} , NaC_{10} , and Na-GIC. Here, the ΔH values are calculated relative to diamond, except when $P = 0$. This is because the enthalpy of diamond is lower than that of graphite at pressures above about 2 GPa. Furthermore, fluorine and sodium undergo structural phase transitions when the pressure is increased,^{44, 45)} so the ΔH of the compounds must be calculated using the enthalpies corresponding to their structures.

For fluorine, the $C2/c$ structure is used for $P < 20$ GPa, and the $Cmca$ structure is used otherwise.⁴⁴⁾ For sodium, the bcc, fcc, $CsIV$, and $P6_3/mmc$ structures are used for $P < 60$, $P = 100$, 200, and 300 GPa, respectively.⁴⁵⁾

The figure indicates that ΔH increases with P for C_6 , C_{10} , FC_{10} , NaC_{10} , and Na-GIC. These substances have relatively low density, so their enthalpy increases under high pressure. In fact, the densities of diamond, C_6 , and C_{10} are 4.64, 3.97, and 3.79 g/cm³, respectively, at $P = 200$ GPa. Furthermore, those of NaC_6 and Na-GIC are 4.18 and 3.54 g/cm³, respectively, at $P = 100$ GPa. Here,

the melting point of Na-GIC is 0 K at $P \sim 110$ GPa, and it may be thermally unstable at pressures above this.

The figure also indicates that the ΔH of NaC_6 decreases with increasing P , while the others generally increase with $P = 0$ except FC_6 . The ΔH of FC_6 seems to be almost independent of P . We have confirmed that the ΔH values for NaC_6 and FC_6 are almost the same at $P = 300$ and 400 GPa. Therefore, it seems that these ΔH values will not decrease even if the pressure is increased further.

In contrast to NaC_6 , the ΔH of NaC_{10} increases with pressure. This can be interpreted as the crystal structure of NaC_{10} being more sparse than that of NaC_6 . This may also apply to the relationship between FC_6 and FC_{10} .

3.5 Formation free energies for NaC_6 and FC_6

As shown in Fig. 9, the ΔH of NaC_6 decreases with increasing pressure and becomes about 0.29 eV at $P = 300$ GPa. In this case, the effects of finite temperature, such as lattice vibrations, may not be negligible near the melting point. To clarify the effects of phonons, we calculate the Helmholtz free energy $F(T)$ by harmonic approximation. Comparing $F(T)$ with experimental results,⁴⁶⁾ we introduce a phenomenologically corrected free energy $\tilde{F}(T)$. It reproduces the experimental results better than $F(T)$ and allows us to estimate the free energy of the liquid state. By adding $\tilde{F}(T)$ to the enthalpy at $T = 0$, we can approximately obtain the Gibbs free energy at finite temperatures. Detailed calculation methods are given in Appendix B.

In Fig. 10(a), we show $\tilde{F}(T)$ as a function of T for diamond, NaC_6 , and sodium at $P = 300$ GPa. We also present the formation free energy, $\Delta\tilde{F}(T)$, which is defined as $\Delta\tilde{F}(T) = \tilde{F}_{\text{NaC}_6}(T) - (\tilde{F}_{\text{Na}}(T) + 6\tilde{F}_{\text{dia}}(T))/7$. Here, $\tilde{F}_{\text{NaC}_6}(T)$, $\tilde{F}_{\text{Na}}(T)$, and $\tilde{F}_{\text{dia}}(T)$ are the $\tilde{F}(T)$ per atom for NaC_6 , sodium, and diamond, respectively. These values decrease with increasing temperature owing to entropy. As shown in the figure, $\Delta\tilde{F}(T)$ is about -0.34 eV at $T = 6550$ K, where this temperature corresponds to T_m of NaC_6 , and T_m of diamond is about 9300 K under the same pressure. Here, to obtain T_m , we used the $N=14$ system for NaC_6 and the $N = 8$ system for diamond.

Recalling that $\Delta H \simeq 0.29$ eV, the value of $\Delta H + \Delta\tilde{F}(T)$ becomes about -0.05 eV. Since the value is negative, we could expect the formation of NaC_6 under this condition.⁴⁷⁾ The result also suggests that high pressure and high temperature may favor the synthesis of NaC_6 .

By applying a similar analysis as described above to FC_6 , $\Delta\tilde{F}(T)$ is about -0.36 eV at $T = 6660$ K, as shown in Fig. 10(b). Here, this temperature corresponds to T_m at $P = 300$ GPa. We assume that $c_{\text{solid}}=1.06$ for fluorine, FC_6 , and diamond. For the liquid state of fluorine, c_{liquid} is assumed to be 1.2. Since the ΔH of FC_6 is about 0.43 eV at $P = 300$ GPa, we obtain $\Delta H + \Delta\tilde{F}(T) \simeq 0.07$ eV. This value is small but positive. Thus, the synthesis of FC_6 may be more difficult than that of NaC_6 .

In the above discussion, we have not address the contribution of electrons at finite temperatures. To consider it, we estimate the free energy of electrons. At $P = 300$ GPa, NaC_6 is metallic and the value of DOS at the Fermi

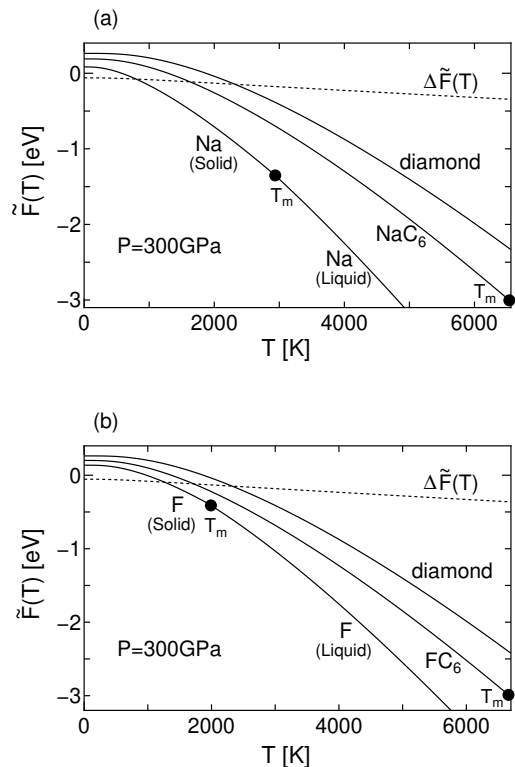


Fig. 10. Free energy as a function of temperature for (a) Na, NaC_6 , and diamond, and (b) F, FC_6 , and diamond at $P = 300$ GPa. Here, solid circles represent T_m . The dotted lines show the formation free energy $\Delta\tilde{F}(T)$, which is determined using a similar definition as ΔH .

level, D_F , is 0.204 states/eV/atom. Using the free electron model, we calculate the contribution of free energy to be $\sim -\frac{\pi^2}{6}(k_B T)^2 D_F$ at low temperatures. The value is about -0.11 eV at $T = 6550$ K. If liquid sodium is in the metallic state, the value of the free energy is expected to be of the same order as NaC_6 . On the other hand, we found that diamond has an energy gap of 5.6 eV at $P = 300$ GPa, and the electron contribution to the free energy is negligible. In this case, the $\Delta\tilde{F}(T)$ of NaC_6 may decrease by about 0.09 eV.

However, we used $\tilde{F}(T)$, which closely reproduces the experimental results. Since the experimental results should include the effect of electrons at finite temperatures, $\tilde{F}(T)$ should be considered to include the effect of electrons, even if it is not complete. If so, adding the electron contribution to $\tilde{F}(T)$ could result in double counting. Similarly, the effects of volume changes at finite temperatures may already be included. In any case, the contribution of these effects may be small and would not significantly change the results.

4. Summary

By combining FPMD method and the Z-method, we investigated the T_m of carbon compounds XC_6 , XC_{10} , and XC_{12} with the sodalite structure. To verify the validity of the method, we apply it to the diamond system and compare the results with those of other theoretical and experimental works. We also discussed the assumptions adopted in the Z-method by comparing them with

experimental results. In addition to the melting points, we obtained the superconducting transition temperature T_c by the optimized tetrahedron method in QE.

These results suggest that FC_6 , FC_{10} , and ClC_{10} can exist stably at sufficiently high temperatures ($T \gtrsim 1000$ K) even under normal pressure, and the T_c values of these compounds reach nearly 100 K. Although the T_m of NaC_6 drops rapidly at pressures below 30 GPa, T_c is over 120 K for $P \gtrsim 30$ GPa. We also showed results for several other compounds that have relatively low T_c but are stable at ambient pressure. If these compounds could actually be synthesized, it would be possible to observe high-temperature superconductivity mediated by phonons.

To examine the feasibility of these compounds, we calculated the formation enthalpies ΔH from the ground state energies of the elements. Unfortunately, all of these values for compounds were positive and above 0.5 eV at $P = 0$. This suggests that the synthesis of these compounds is not easy. We also examined the pressure dependence of ΔH for C_6 , C_{10} , and several representative compounds. Since C_6 and C_{10} have lower densities than diamond, ΔH increases with pressure. However, the ΔH of NaC_6 decreases with increasing pressure, from about 0.94 eV at $P = 0$ to 0.29 eV at $P = 300$ GPa.

In this case, the effect of finite temperature may make the Gibbs formation free energy negative. To clarify this, we introduced a phenomenologically corrected formation free energy $\Delta\tilde{F}(T)$. Applying this to NaC_6 , we found the value of $\Delta\tilde{F}(T)$ to be approximately -0.36 eV at $T = 6600$ K and $P = 300$ GPa. This cancels out the positive ΔH , and $\Delta\tilde{F}(T) + \Delta H$, which corresponds to the Gibbs formation free energy, becomes negative.

This result suggests that sufficiently high temperatures and pressures may be effective for the formation of NaC_6 . Applying a similar analysis to FC_6 , we found that the Gibbs formation free energy is small but positive under conditions similar to those for NaC_6 . This result indicates that the synthesis of FC_6 may be more difficult than that of NaC_6 .

ACKNOWLEDGMENTS

This work was supported by JSPS KAKENHI Grant Number JP19K03716.

Appendix A: Z-method

The result of the Z-method is derived under the basic assumption $U_{\text{solid}}(T_u) = U_{\text{liquid}}(T_m)$, where $U_{\text{solid}}(T)$ and $U_{\text{liquid}}(T)$ are the internal energies of the system in the solid and liquid states, respectively. Moreover, two approximate relations, $C_V(T_m) \simeq 3k_B$ and $\Delta S \simeq k_B \ln 2$, are used,⁴⁸⁾ where $C_V(T_m)$ is the specific heat at constant volume in the solid state at T_m , and ΔS is the entropy change between the liquid and solid states.⁴⁹⁾ These lead to $T_u/T_m = (1 + \Delta S/C_V(T_m)) \simeq 1.23$.²⁸⁾

The first assumption is based on the results of MD simulations and seems plausible. To confirm the validity of the second relations, we compare them with experimental results, where the difference between $C_V(T_u)$ and $C_P(T_u)$ is neglected. Table A-1 gives these experimental values with melting points T_m^{ex} for several elements and compounds below.⁵⁰⁾ For reference, our calculated results

of T_m are also added.

Table A-1. Experimental data for C_p , ΔS , $\Delta S/C_p$, and T_m^{ex} together with calculated T_m

	Na	Ca	Al	NaCl	B ₄ C	Be ₂ C
C_p/k_B	3.80	5.20	3.96	4.05	3.79	3.69
$\Delta S/k_B$	0.844	0.921	1.38	1.58	0.917	1.26
$\Delta S/C_p$	0.222	0.177	0.242	0.389	0.242	0.341
$T_m^{\text{ex}50)}$ [K]	371	1115	933	1074	2743	2400
T_m [10^3 K]	0.36	1.2	0.94	0.90	3.0	2.7
size (N)	16	32	4	8	45	12

Although the experimental values of C_p/k_B and $\Delta S/k_B$ ⁵⁰⁾ are larger than the theoretically expected values, the values of $1 + \Delta S/C_p$ are relatively close to 1.23. The above results suggest that the equation $T_m = T_u/1.23$ is a reasonable approximation even for compounds.

To consider the validity of T_m , we present some additional results on T_m below. It is 431 K for Na with $N = 54$, 1504 K for Ca with $N=4$, and 585 K for Al with $N = 32$. The results show that the size dependence of T_m is not very consistent, and T_m for larger systems do not necessarily give better values. Although it may be difficult to precisely estimate T_m by this method, it is possible to obtain the approximate T_m of complex systems such as compounds with a small amount of calculation.

Appendix B: Free Energy

We consider the Helmholtz free energy $F(T)$ per atom within the harmonic approximation for phonons. In the harmonic approximation, the volume of the system does not depend on T . Thus, we neglect the volume change of the system due to temperature hereafter.

Using the free energy formulation for a harmonic oscillator, we obtain

$$F(T) = \int \left[\frac{\hbar\omega}{2} + k_B T \ln(1 - \exp(-\frac{\hbar\omega}{k_B T})) \right] \rho_{\text{ph}}(\omega) d\omega,$$

where $\rho_{\text{ph}}(\omega)$ is the phonon DOS per atom, which can be calculated by QE. The internal energy $U(T)$ can also be obtained by a similar formulation as

$$U(T) = \int \frac{\hbar\omega}{2} \left[1 + \frac{1}{\exp(\frac{\hbar\omega}{k_B T}) - 1} \right] \rho_{\text{ph}}(\omega) d\omega.$$

Here, entropy $S(T)$ can be easily obtained by $S(T) = (U(T) - F(T))/T$.

To compare the experimental results with the above results, we consider the enthalpy of phonons, $H(T)$. Since the pV term is already included in the enthalpy calculated for the electron system, there is no need for it in $H(T)$. Therefore, $H(T)$ is equivalent to $U(T)$ for phonons. Since enthalpy is typically used in experiments,⁵⁰⁾ we use $H(T)$ instead of $U(T)$ to avoid confusion.

As shown in Fig. B-1(a), we find that the experimental result of the enthalpy $H^{\text{ex}}(T)$ for sodium⁵⁰⁾ is well fitted by $H^{\text{ex}}(T) \simeq c_{\text{solid}}H(T)$ for $T \leq T_m$ and $H^{\text{ex}}(T) \simeq c_{\text{liquid}}H(T) + \Delta_g$ for $T > T_m$, where c_{solid} is a

constant, 1.06, and c_{liquid} is 1.19. Here, Δ_g is the value to reproduce the gap in $H^{\text{ex}}(T)$ at T_m , which will be given later. For the case of NaCl,⁵⁰ we obtain $c_{\text{solid}} = 1.06$ and $c_{\text{liquid}} = 1.28$, as shown in Fig. B-1(b). The c_{solid} values are the same for Na and NaCl, but the c_{liquid} values are slightly different.

As shown in Figs. B-1(c) and B-1(d), we find that similar relationships hold for entropies. That is, $S^{\text{ex}}(T) \simeq c_{\text{solid}}S(T)$ for $T < T_m$ and $S^{\text{ex}}(T) \simeq c_{\text{liquid}}S(T)$ for $T \geq T_m$. These relations lead to $\tilde{F}(T) \simeq c_{\text{solid}}F(T)$ for $T < T_m$ and $\tilde{F}(T) \simeq c_{\text{liquid}}F(T) + \Delta_g$ for $T \geq T_m$, where $\tilde{F}(T)$ is the phenomenologically corrected free energy that is fitted to closely reproduce the experimental results, and $\Delta_g = (c_{\text{solid}} - c_{\text{liquid}})F(T_m)$.

The above phenomenological relations give approximate free energies of the solid and liquid states which closely reproduce the experimental results. The results of Figs. B-1 suggest that this approximation can be widely applied to a variety of materials. In fact, we confirmed that this method can also be applied to Al and B₄C.⁵⁰ We found that $c_{\text{solid}} = 1.09$ and $c_{\text{liquid}} = 1.3$ in the former case. In the latter case, $c_{\text{solid}} = 1.03$ and $c_{\text{liquid}} = 1.13$.

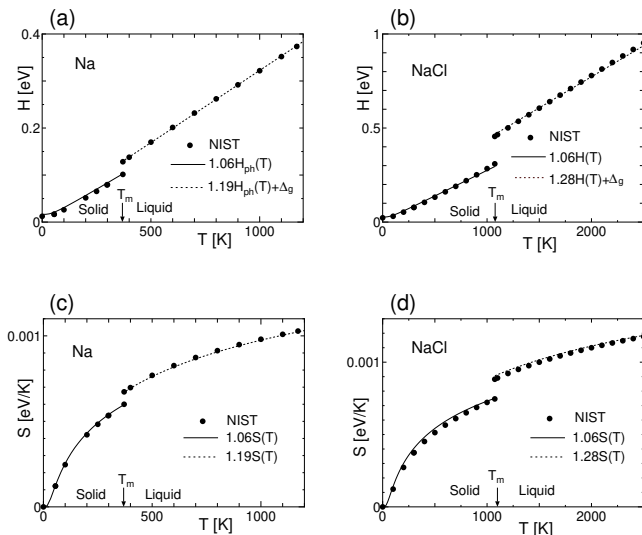


Fig. B-1. Theoretical and experimental results of enthalpy as a function of T for (a) Na and (b) NaCl, and those of entropy for (c) Na and (d) NaCl, where the experimental results are taken from NIST.⁵⁰ Here, the experimental values of enthalpy are shifted by a constant to match the theoretical value of $H(T)$ at $T = 0$.

To test the above analysis, we tried to find the phase boundary between graphite and diamond. When $T = 0$, the enthalpy of diamond is lower than that of graphite and diamond is stable for $P \gtrsim 2$ GPa.^{38, 51} As the temperature increases, the free energy of graphite decreases more quickly than that of diamond, and graphite becomes stable. The boundary is given by $\Delta\tilde{F}(T) + \Delta H = 0$, where $\Delta\tilde{F}(T)$ and ΔH are the formation free energy and the formation enthalpy of graphite, respectively.

In Fig. B-2, we show the $\tilde{F}(T)$ of diamond and graphite and $\Delta\tilde{F}(T)$ of graphite, where c_{solid} is set to 1.06 for both diamond and graphite. Here, we confirmed that the $\tilde{F}(T)$

of graphite almost reproduces the experimental result.⁵⁰ In the figure, the solid lines represent the $\tilde{F}(T)$ of diamond and graphite at $P = 8$ GPa. $\Delta\tilde{F}(T)$ is shown as a dotted line for $P = 8$ GPa and as a dashed line for $P = 15$ GPa. The two lines are close to each other and look nearly identical. The result indicates that the P -dependence of $\Delta\tilde{F}(T)$ is very small. On the other hand, the P -dependence of ΔH is not so small and dominates the conditions that determine the phase boundary.

The ΔH values are -0.129 , -0.0283 , 0.0318 , 0.0514 , and 0.1293 for $P = 0, 5, 8, 10$, and 15 GPa, respectively. Using the results above, we found that the boundary temperatures are approximately 0, 750, 1300, and 3400 K for $P = 6.9, 8, 10$, and 15 GPa, respectively. This boundary appears to be shifted by about 5 GPa toward higher pressure compared with other theoretical⁵¹ and experimental³⁸ results. Apart from this, the result seems to agree with those of other works.

The application to the boron-doped diamond system is also interesting. It is synthesized at high pressure (~ 10 GPa) and temperature (~ 3000 K) and shows superconductivity with $T_c \sim 4$ K.¹² Here, the boron concentration, ρ_b is about 3 percent. In Fig. B-3, we show the $\tilde{F}(T)$ of diamond, boron-doped diamond, and boron at $P = 10$ GPa. For boron-doped diamond, we use the $N = 32(4 \times 4 \times 2)$ system, in which one atom is replaced by boron.

In a real system, the effect of entropy becomes important⁵² because the boron atoms are randomly distributed in the system. We evaluated the additional en-

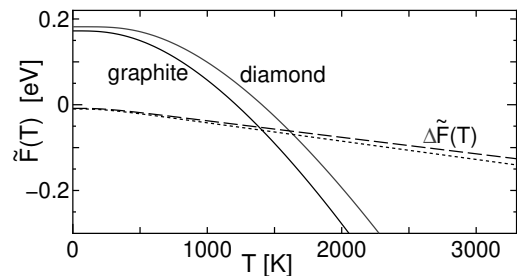


Fig. B-2. Phenomenological free energies, $\tilde{F}(T)$ of diamond and graphite (solid lines) at $P = 8$ GPa, together with the formation free energies $\Delta\tilde{F}(T)$ of graphite at $P = 8$ (dotted line) and $P = 15$ GPa (dashed line).

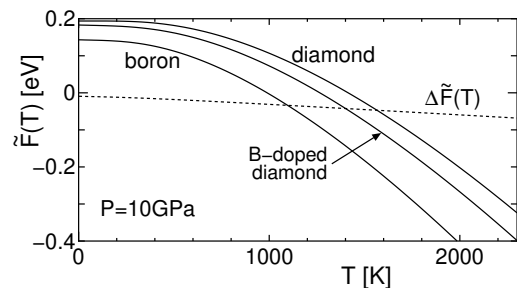


Fig. B-3. Phenomenological free energies, $\tilde{F}(T)$ of diamond, boron, and boron-doped diamond at $P = 10$ GPa (solid lines). The formation free energy $\Delta\tilde{F}(T)$ of boron-doped diamond is represented by a dotted line.

entropy by treating the boron-doped system as a type of binary alloy.⁵³⁾ In this case, the entropy is expressed as $-k_B(\rho_b \ln \rho_b + (1 - \rho_b) \ln(1 - \rho_b))$. For $\rho_b = 0.03$, the value is $\simeq 0.12 \times 10^{-4}$ eV/K, and we add it to the $\tilde{F}(T)$ of the boron-doped diamond.

In this figure, the dotted line indicates the formation free energy $\Delta\tilde{F}(T)$ of boron-doped diamond. Here, to obtain $\Delta\tilde{F}(T)$, we assume that the crystal structure of boron is $R\bar{3}m$.^{43, 54)} It decreases with increasing temperature, and $\Delta\tilde{F}(T) + \Delta H$ becomes negative at $T \gtrsim 1200$ K. Here, ΔH is the formation enthalpy of boron-doped diamond, and its value is about 0.038 eV. This result means that the boron-doped diamond is stable at $T \gtrsim 1200$ K.⁵⁵⁾ It does not contradict the synthesis conditions of the boron-doped diamond.¹²⁾

As mentioned above, our evaluation of the free energy is expected to be useful in finding conditions for material synthesis. To analyze the free energy of NaC₆, we use $c_{\text{solid}} = 1.06$ and $c_{\text{liquid}} = 1.13$ as the phenomenological parameters for sodium at $P = 300$ GPa. For simplicity, we also use $c_{\text{solid}} = 1.06$ for diamond and NaC₆. The calculated results are given in the main text.

- 1) H. Wang, J. S. Tse, K. Tanaka, T. Iitaka, and Y. Ma, Proc. Natl. Acad. Sci. USA **109**, 6463 (2012).
- 2) X. Feng, J. Zhang, G. Gao, H. Liu, and H. Wang, RSC Adv. **5**, 59292 (2015).
- 3) Y. Li, J. Hao, H. Liu, J. S. Tse, Y. Wang and Y. Ma, Sci. Rep. **5** 9948 (2015).
- 4) H. Liu, I. I. Naumov, R. Hoffmann, N. W. Ashcroft, and R. J. Hemley, Proc. Natl. Acad. Sci. USA **114**, 6995 (2017).
- 5) F. Peng, Y. Sun, C. J. Pickard, R. J. Needs, Q. Wu, and Y. Ma Phys. Rev. Lett. **119**, 107001 (2017).
- 6) C. Heil, S. di Cataldo, G. B. Bachelet, and L. Boeri Phys. Rev. B **99**, 220502(R) (2019).
- 7) I. A. Kruglov, D. V. Semenok, H. Song, R. Szczesniak, I. A. Wrona, R. Akashi, M. M. D. Esfahani, D. Duan, T. Cui, A. G. Kvashnin, and A. R. Oganov, Phys. Rev. B **101**, 024508 (2020).
- 8) A. P. Drozdov, P. P. Kong, V. S. Minkov, S. P. Besedin, M. A. Kuzovnikov, S. Mozaffari, L. Balicas, F. F. Balakirev, D. E. Graf, V. B. Prakapenka, E. Greenberg, D. A. Knyazev, M. Tkacz, and M. I. Erements Nature **569** 528 (2019)
- 9) M. Somayazulu, M. Ahart, A. K. Mishra, Z. M. Geballe, M. Baldini, Y. Meng, V. V. Struzhkin, and R. J. Hemley, Phys. Rev. Lett. **122**, 027001 (2019).
- 10) I. A. Troyan, D.V. Semenok, A.G. Kvashnin, A.G. Ivanova, V.B. Prakapenka, E. Greenberg, A.G. Gavriliuk, I.S. Lyubutin, V.V. Struzhkin, and A.R. Oganov, Adv. Mater. **33** 2006832 (2021).
- 11) P. P. Kong, V. S. Minkov, M. A. Kuzovnikov, S. P. Besedin, A. P. Drozdov, S. Mozaffari, L. Balicas, F.F. Balakirev, V. B. Prakapenka, E. Greenberg, D. A. Knyazev, and M. I. Erements, Nat. Commun. **12**, 5075 (2021).
- 12) E. A. Ekimov, V. A. Sidorov, E. D. Bauer, N. N. Mel'nik, N. J. Curro, J. D. Thompson, and S. M. Stishov, Nature **428**, 542 (2004).
- 13) Y. Ma, J. S. Tse, T. Cui, D. D. Klug, L. Zhang, Y. Xie, Y. Niu, and G. Zou, Phys. Rev. **B72**, 014306 (2005).
- 14) A. Kawano, H. Ishikawa, S. Iriyama, R. Okada, T. Yamaguchi, Y. Takano, and H. Kawarada, Phys. Rev. B **82**, 085318 (2010).
- 15) H. Okazaki, T. Wakita, T. Muro, T. Nakamura, Y. Muraoka, T. Yokoya, S. Kurihara, H. Kawarada, T. Oguchi, and Y. Takano, Appl. Phys. Lett. **106**, 052601 (2015).
- 16) T. E. Weller, M. Ellerby, S. S. Saxena, R. P. Smith, and N. T. Skipper, Nat. Phys. **1**, 39 (2005).
- 17) R. P. Smith T. E. Weller, C. A. Howard, M. P.M. Dean, K. C. Rahnejat, S. S. Saxena, and M. Ellerby, Physica C **514**, 50 (2015).
- 18) C. M. Hao, X. Li , A.R. Oganov, J. Hou, S. Ding, Y. Ge, L. Wang, X. Dong, H. T. Wang, G. Yang, X. F. Zhou, and Y. Tian, Phys. Rev. B **108**, 214507 (2023).
- 19) A. P. Ramirez, Physica C **514**, 166 (2015).
- 20) S. Lu, H. Liu, I. I. Naumov, S. Meng, Y. Li, J. S. Tse, B. Yang, and R. J. Hemley, Phys. Rev. **B93**, 104509 (2016). See also their supplemental materials.
- 21) Q. Wei, Q. Zhang, and M. Zhang, Materials **9**, 726 (2016).
- 22) K. Sano, Y. Masuda, and H. Ito, J. Phys. Soc. Jpn. **91**, 083703 (2022).
- 23) N. S. Khan, B. R. Rano, I. M. Syed, R.S. Islam, and S.H. Naqib, Results Phys. **33**, 105182 (2022).
- 24) Y. L. Hai, M. J. Jiang, H. L. Tian, G. H. Zhong, W. J. Li, C. L. Yang, X. J. Chen, and H. Q. Lin, Adv. Sci. **10**, 2303639 (2023).
- 25) S. Jin, X. Kuang, X. Dou, A. Hermann, and C. Lu J. Mater. Chem. C **12**, 1516 (2024).
- 26) A. Pokropivny and S. Volz, Phys. Status Solidi B **249**, 1704 (2012).
- 27) P. Giannozzi, S. Baroni, N. Bonini, M. Calandra, R. Car, C. Cavazzoni, D. Ceresoli, G. L. Chiarotti, M. Cococcioni, I. Dabo, A. Dal Corso, S. Fabris, G. Fratesi, S. de Gironcoli, R. Gebauer, U. Gerstmann, C. Gougoussis, A. Kokalj, M. Lazzeri, L. Martin-Samos, N. Marzari, F. Mauri, R. Mazzarello, S. Paolini, A. Pasquarello, L. Paulatto, C. Sbraccia, S. Scandolo, G. Sclauzero, A. P. Seitsonen, A. Smogunov, P. Umari, and R. M. Wentzcovitch, J. Phys. Condens. Matter **21**, 395502 (2009).
- 28) A. B. Belonoshko, N. V. Skorodumova, A. Rosengren, and B. Johansson, Phys. Rev. B **73**, 012201 (2006).
- 29) A. R. Finneya and P. M. Rodger, Phys. Chem. Chem. Phys. **13**, 19979 (2011).
- 30) S. Wang, G. Zhang, H. Liu, and H. Song, J. Chem. Phys. **138**, 134101 (2013).
- 31) H. Y. Geng, R. Hoffmann, and Q. Wu, Phys. Rev. B **92**, 104103 (2015).
- 32) F. A. Lindemann, Z. Phys. **11**, 609 (1910).
- 33) M. Ross, Phys. Rev. **184**, 233 (1969).
- 34) J. N. Shapiro, Phys. Rev. B **1**, 3982 (1970).
- 35) Z. H. Jin, P. Gumbsch, K. Lu, and E. Ma, Phys. Rev. Lett. **87**, 055703 (2001).
- 36) X. F. Wang, S. Scandolo, and R. Car, Phys. Rev. Lett. **95**, 185701 (2005).
- 37) A. A. Correa, S. A. Bonev, and G. Galli, Proc. Natl. Acad. Sci. USA **103**, 1204 (2006).
- 38) F. P. Bundy, W. A. Bassett, M. S. Weathers, R. J. Hemley, H. K. Mao, and A. F. Goncharov, Carbon **34**, 141 (1996).
- 39) A. Liang, Y. Liu, L. Shi, L. Lei, F. Zhang, Q. Hu, and D. He, Phys. Rev. Res. **1**, 033090 (2019).
- 40) P. B. Allen and R. C. Dynes, Phys. Rev. B **12**, 905 (1975).
- 41) The transition temperature T_c is calculated using the Allen and Dynes formulation,⁴⁰⁾ where the screened Coulomb potential parameter μ^* is set to 0.1 as a typical value. We found that $T_c \simeq 259K$ for YH₆ at $P = 166$ GPa, while the experimental result at the same pressure is 224 K.^{10, 11)} For LaH₁₀, T_c is estimated to be 212 K at $P = 220$ GPa, but it is 245 K in the experimental results.^{8, 9)} Here, \mathbf{k} mesh (\mathbf{q} mesh) is chosen to be $8 \times 8 \times 8$ ($4 \times 4 \times 4$). The mesh of electron-phonon calculation is chosen to be $16 \times 16 \times 16$. We confirmed that the results of T_c are almost the same even if the meshes are different.
- 42) C.S. Sundar, A. Bharathi, Y. Hariharan, J. Janaki, V.S. Sastry, and T.S. Radhakrishnan, Solid State Commun. **84**, 823 (1992).
- 43) A. Jain, S. P. Ong, G. Hautier, W. Chen, W. D. Richards, S. Dacek, S. Cholia, D. Gunter, D. Skinner, G. Ceder, and K. A. Persson, APL Mater. **1**, 011002 (2013). www.materialsproject.org
- 44) C. Tantardini, F. N. Jalolov, and A. G. Kvashnin, J. Phys. Chem. C **126**, 11358 (2022).
- 45) N. E. Christensen and D. L. Novikov, Solid State Commun.

- 119, 477 (2001).
- 46) Y. Huang, M. Widom, and M. C. Gao, *Phys. Rev. Mater.* **6**, 013802 (2022).
- 47) To precisely discuss the synthesis conditions, it may be necessary to improve the accuracy of ΔH . Additionally, the presence of other compounds such as NaC may need to be considered.
- 48) If the simulations can be performed in sufficient detail, it is possible to determine T_m without using these two approximate relations.
- 49) S. M. Stishov, *Usp. Fiz. Nauk* **114**, 3 (1974).
- 50) National Institute of Standards and Technology Federal Information Processing Standards Publications, **140**, 2 (2002) <https://janaf.nist.gov/>
- 51) L. M. Ghiringhelli, J. H. Los, E. J. Meijer, A. Fasolino, and D. Frenkel, *Phys. Rev. Lett.* **94**, 145701 (2005).
- 52) A. Manzoor, S. Pandey, D. Chakraborty, S. R. Phillpot, and D. S. Aidhy, *npj Comput. Mater.* **4**, 47 (2018).
- 53) For a binary alloy, a lattice gas model is often used as a simple approximation. See below its the entropy formula. G. D. With, *Liquid-State Physical Chemistry: Fundamentals, Modeling, and Applications* (Wiley-VCH Verlag GmbH & Co. KGaA, 2013) Appendix C.
- 54) G. Parakhonskiy, N. Dubrovinskaia, L. Dubrovinsky, S. Mondal, and S. v. Smaalen, *J. Cryst. Growth* **321**, 162 (2011).
- 55) We confirmed that these results are almost unchanged even if the existence of B_4C is taken into account.